

## Charge Separation of Dense Two-Dimensional Electron-Hole Gases: Mechanism for Exciton Ring Pattern Formation

R. Rapaport,<sup>1</sup> Gang Chen,<sup>1</sup> D. Snoke,<sup>2</sup> Steven H. Simon,<sup>1</sup> Loren Pfeiffer,<sup>1</sup> Ken West,<sup>1</sup> Y. Liu,<sup>2</sup> and S. Denev<sup>2</sup>

<sup>1</sup>*Bell Laboratories, Lucent Technologies, 600 Mountain Avenue, Murray Hill, New Jersey 07974, USA*

<sup>2</sup>*Department of Physics and Astronomy, University of Pittsburgh, 3841 O'Hara Street, Pittsburgh, Pennsylvania 15260, USA*

(Received 29 August 2003; published 18 March 2004)

We report on new experiments and theory that unambiguously resolve the recent puzzling observation of large diameter exciton emission halos around a laser excitation spot in two dimensional systems. We find a novel separation of plasmas of opposite charge with emission from the sharp circular boundary between these two regions. This charge separation allows for cooling of initially hot optically generated carriers as they dwell in the charge reservoirs for very long times.

DOI: 10.1103/PhysRevLett.92.117405

PACS numbers: 78.67.-n, 78.55.-m

The search for Bose-Einstein condensation (BEC) of excitons in semiconductors has attracted intense research for decades and is still an ongoing effort. Indirect excitons in double quantum well (QW) structures are thought of as good candidates for observing such a phenomenon. Nevertheless, clear and convincing evidence for excitonic BEC is yet to be demonstrated. Recently, Butov *et al.* [1] and Snoke *et al.* [2] independently studied the emission from modulation doped double QW structures under optical excitation from a tightly focused laser beam. When voltage is applied in the growth direction, emission is observed from the indirect excitons. Imaging the spatial distribution of this emission reveals a surprising pattern: in addition to the expected emission at the excitation spot, an emission ring is seen at large radial distances, with a dark region in between the center spot and the ring. It was initially speculated that this effect is strongly related to the long sought excitonic BEC. However, those initial speculations seem inconsistent with many experimental results [3]. It is obvious that there is transport of particles from the excitation spot to the remote ring over macroscopic distances. The key questions are what types of particles are transported through the dark region and what is the driving force? In this Letter we unambiguously identify an optically induced in-plane separation of oppositely charged plasmas as the underlying physical mechanism. The separated charges form an extremely persistent and sharp circular boundary where a dense gas of excitons is formed, giving rise to the ring emission pattern.

One of the first key clues for solving this problem is our observation that identical ring patterns are also seen in single quantum well structures, as opposed to the double QW structures studied in the initial reports [1,2]. In these structures, there are only direct excitons, which implies that the effect does not depend on the specific characteristics of indirect excitons (such as long lifetimes) as was suggested previously. Another important clue can be found in the observed excitation energy threshold of the ring formation: the ring easily forms only with photo-

excitation energies above the AlGaAs barrier band gap energy [4]. Since it is known that in modulation doped structures, optical excitation above the barriers can lead to depletion of electrons [5], the mechanism responsible for the ring formation might have to do with such optical depletion. It is then sensible to obtain further insight into the above mentioned questions by performing careful spectroscopic studies. The line shapes, linewidths, and energies of the emission from the center spot and the ring are very good local probes of the carrier density distributions in the QW plane.

Figures 1(a)–1(c) show the ring pattern from our single well sample [6] at various excitation powers. As shown in Fig. 2(a), the ring radius grows (sublinearly) with

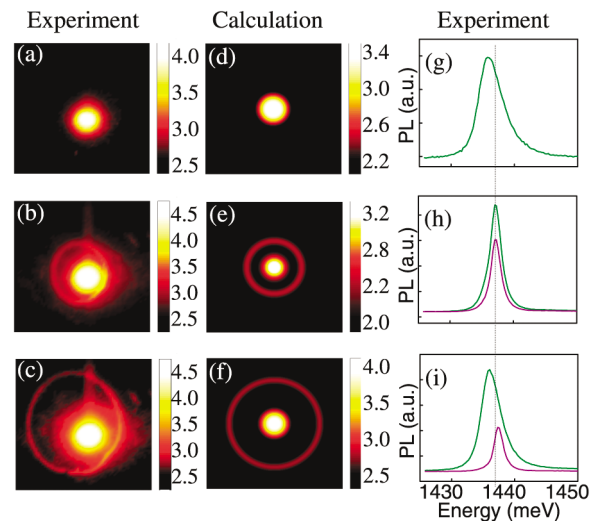


FIG. 1 (color). Photoluminescence images for our single QW sample taken at excitation powers of 50, 265, and 296  $\mu\text{W}$ , are shown in the left panel (a)–(c). The middle panel (d)–(f) shows the results of the model calculations. All images are  $700 \times 700 \mu\text{m}$ . The right panel (g)–(i) presents the experimentally observed center spot (olive) and ring (purple) emission spectra. The sample was measured at  $T = 8 \text{ K}$ , and excited with a HeNe laser (632 nm) with a spot diameter of  $\sim 60 \mu\text{m}$ .

increasing excitation power above a certain critical threshold for ring creation. Figures 1(g)–1(i) show the center spot and ring PL spectra corresponding to Figs. 1(a)–1(c). The detailed behavior of the spectral linewidth and energy as a function of excitation power is shown in Figs. 2(b) and 2(c) for both the center spot and the ring. From Figs. 2(b) and 2(c), we see the following trend: At low excitation power, there is no ring and the emission of the center spot is broad, asymmetric, and redshifted [see also Fig. 1(g)], as expected from emission from a region with a high density of dissociated charge carriers. As the power is increased, the linewidth of the central spot narrows by a factor of 2, becomes more symmetric, and less redshifted compared to the center spot at lower intensity. Since the line is symmetric and narrow, we believe this to be the emission of a gas of excitons [see Fig. 1(h)] [7]. As the power is further increased and the radius of the ring grows, the spectrum of the center spot redshifts, broadens, and becomes asymmetric [see also Fig. 1(i)], indicative of a gas of dissociated carriers again. In contrast, the spectrum of the ring remains nearly constant: unshifted, symmetric, and narrow, indicative of a gas of excitons. Finally, Fig. 2(d) plots the peak PL intensities as a function of power. The center spot emission increases with power, except for a sudden drop around the threshold for ring creation. The ring intensity, on the other hand, drops with increasing power (and corresponding increasing radius).

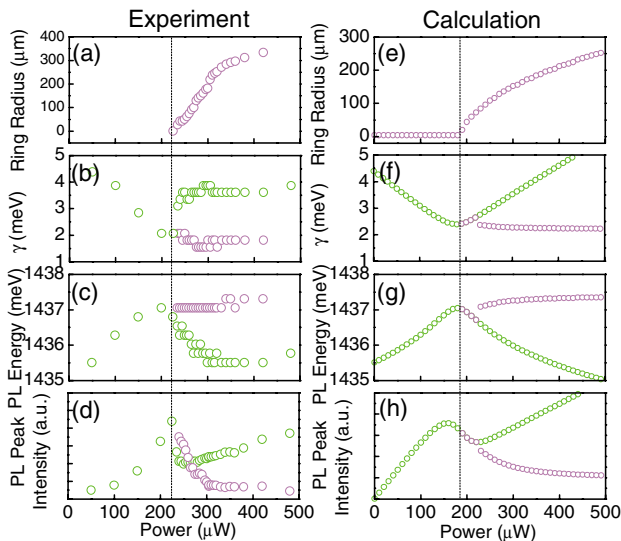


FIG. 2 (color). Comparison between the experimental and model calculated excitation power dependences: (a) experimental and (e) calculated ring radius; (b) the measured linewidth and (c) the energy of the center spot luminescence (olive circles) and the ring luminescence (purple circles); (f) model calculated linewidth of the luminescence of the center spot and ring assuming degenerate 2D electron-hole plasma; (g) model calculated energies of the center spot and ring luminescence based on band gap renormalization; (d) experimental and (h) calculated PL peak intensity at the center spot and the ring. Vertical dashed lines mark the onset of the ring formation.

117405-2

We now try to construct a consistent physical picture to account for all of our experimental results. Figure 3(a) shows a schematic description of the relevant processes associated with above-the-barrier photoexcitation, under an applied bias in the growth direction. Without photoexcitation, a 2D electron gas is present in the QW due to the modulation doping of the sample, and its density depends on the leakage current. When hot electrons and holes are photogenerated by the laser, as shown by the red and blue dots in Fig. 3(a), they can either drift under the applied bias to the contacts or cool down through phonon-carrier or carrier-carrier scattering, and consequently get trapped in the QW (red and blue open circles). However, the trapping rate of holes is expected to be larger than that of the electrons since the hole has a much smaller drift velocity (by a factor of 10–20 [8]) and a shorter phonon scattering time [9] than the electron. This results in the hot holes cooling faster (and drifting slower). As a consequence, there is an excess of photogenerated holes that

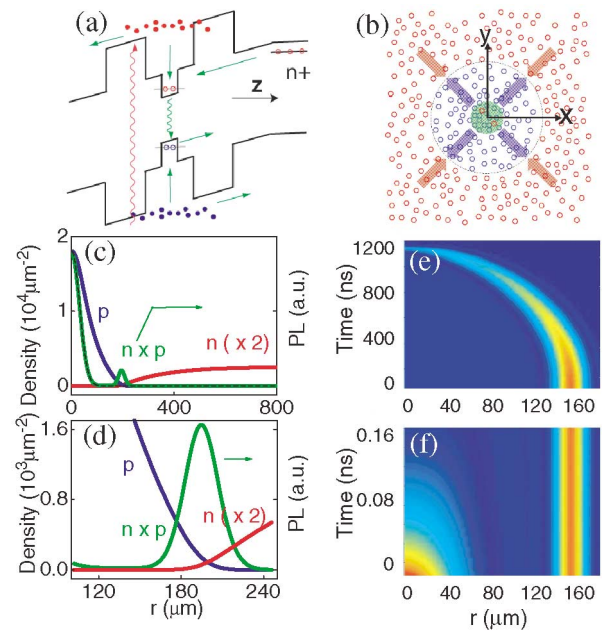


FIG. 3 (color). (a) The energy profile of the QW structure in the growth direction and the relevant electronic processes under photoexcitation (see text). (b) Schematic description of in-plane distributions of cold electrons (open red circles) and excess cold holes (open blue circles) under steady state. The excitation spot is marked by the shaded circular area. The recombination of electrons and holes at the boundary gives rise to the ring pattern. (c) Calculated cold electron (red) and hole (blue) density profiles and the PL intensity (olive) profile for a CW excitation at a power of  $350 \mu\text{W}$ . The black dashed line shows the incident photon intensity radial profile. (d) is an expanded view of (c) around the ring position. (e) Calculated emission pattern cross section as a function of time after the excitation power is turned off. The ring PL and radius decay on a time scale of a microsecond. (f) An expanded view of (e) for very short times immediately after the power is turned off showing that the center spot PL decays on a time scale of picoseconds.

117405-2

end up trapped in the QW. These holes will recombine with the electron gas in the QW, thus depleting it. The degree of depletion depends on the photogeneration rate compared to the leakage rate from the contacts which can replenish the electron density. With high enough excitation power, the electron gas near the illumination spot can be almost completely depleted, leaving a local population of trapped cold holes instead. As a result, close to the center spot, there will be a puddle of holes, surrounded by a sea of electrons. Because of diffusion, the holes tend to spread outwards, while the electrons will flow inwards. This process is schematically shown in Fig. 3(b). In steady state, the holes and electrons are spatially separated in the plane of the QW, *perpendicular* to the applied electric field, forming a sharp (nominally circular) boundary which extends to a radius larger than that of the excitation spot. Since electrons and holes can only recombine where they meet, a sharp luminescence ring will form at the boundary between the two regions of opposite charges.

With this physical picture, the dynamics of the carriers in the QW plane can be described using the following coupled rate equations:

$$\frac{\partial n_{\text{hot}}}{\partial t} = D_{\text{hot}}^e \nabla^2 n_{\text{hot}} - \frac{n_{\text{hot}}}{\tau_{\text{cool}}^e} - \frac{n_{\text{hot}}}{\tau_{\text{drift}}^e} + Af(r), \quad (1)$$

$$\frac{\partial p_{\text{hot}}}{\partial t} = D_{\text{hot}}^h \nabla^2 p_{\text{hot}} - \frac{p_{\text{hot}}}{\tau_{\text{cool}}^h} - \frac{p_{\text{hot}}}{\tau_{\text{drift}}^h} + Af(r), \quad (2)$$

$$\begin{aligned} \frac{\partial n_{\text{cold}}}{\partial t} = & D_{\text{cold}}^e \nabla^2 n_{\text{cold}} + \frac{n_{\text{hot}}}{\tau_{\text{cool}}^e} - \frac{n_{\text{cold}} - n_{\text{eq}}}{\tau_{\text{leak}}^e} \\ & - \xi n_{\text{cold}} p_{\text{cold}}, \end{aligned} \quad (3)$$

$$\frac{\partial p_{\text{cold}}}{\partial t} = D_{\text{cold}}^h \nabla^2 p_{\text{cold}} + \frac{p_{\text{hot}}}{\tau_{\text{cool}}^h} - \frac{p_{\text{cold}}}{\tau_{\text{leak}}^h} - \xi n_{\text{cold}} p_{\text{cold}}. \quad (4)$$

The first two equations describe the dynamics of the density distributions of hot electrons  $n_{\text{hot}}(\vec{r})$  and hot holes  $p_{\text{hot}}(\vec{r})$  in the plane. The first term on the right-hand side of these equations allows them to diffuse with diffusion constants  $D_{\text{hot}}^e$  and  $D_{\text{hot}}^h$  (the  $\nabla^2$  are derivatives in the in-plane directions only). The next two terms on the right-hand side allow them to cool with characteristic times  $\tau_{\text{cool}}^e$  and  $\tau_{\text{cool}}^h$ , respectively, or to drift to the contacts with times  $\tau_{\text{drift}}^e$  and  $\tau_{\text{drift}}^h$ . Finally, we have added the source term  $Af(r)$  which creates hot electrons and holes from photons. Here,  $f(r)$  is the normalized excitation beam profile and  $A$  is the total absorbed photon flux (each absorbed photon generates one electron and one hole). Similarly, the third and fourth equations describe the dynamics of the density distributions of cold electrons  $n_{\text{cold}}(\vec{r})$  and cold holes  $p_{\text{cold}}(\vec{r})$  in the plane. Again, the first term on the right-hand side allows the cold electrons and holes to diffuse with diffusion constants  $D_{\text{cold}}^e$  and  $D_{\text{cold}}^h$ . The second term on the right-hand side generates cold

carriers from any hot carriers that are cooled down. The third term on the right-hand side allows the cold carriers to leak to or from the contacts with rates  $\tau_{\text{leak}}^e$  and  $\tau_{\text{leak}}^h$ , respectively, in a way that tries to bring the densities back to the densities of the dark state ( $n_{\text{eq}}$  for electrons, and zero for holes). Finally, the last term on the right-hand side represents the recombination of cold carriers, where  $\xi$  is the electron-hole capture coefficient.

The steady state solutions of the model are presented in Figs. 3(c) and 3(d) for a set of experimentally determined parameters discussed in detail in Ref. [6] and at an excitation power level where a ring is formed. The laser intensity profile is shown by the black dashed line. The in-plane cold electron and hole density distribution profiles are shown by the red and blue lines, respectively. Consistent with our qualitative picture, the model predicts that both the electron depletion region and the puddle of holes are larger than the excitation spot due to the diffusion processes. The olive line shows the emission profile, which is just the product of the cold electron and cold hole densities. The emission ring appears at the sharp boundary between the electron sea and the hole puddle. The calculated emission patterns corresponding to the experimental conditions of Figs. 1(a)–1(c) are plotted in Figs. 1(d)–1(f). There is a good agreement between the experiment and calculation except for the experimental asymmetry of the ring with respect to the center spot. We attribute this asymmetry to a gradient of barrier width, which is not taken into account in our model. As the barrier width changes there will be corresponding changes in  $n_{\text{eq}}$  causing the ring radius to locally vary.

In order to check the validity and consistency of our model, we compare its predictions to our spectroscopic experimental findings in Fig. 2. First, as the excitation power is increased above a threshold, the electron depletion region and the area of the hole puddle increase. This pushes the ring away from the center spot. This behavior is well reproduced by the model, as seen in Fig. 2(e). The second crucial test of our physical picture is its ability to explain the puzzling dependence on excitation power of the linewidth and energy of the PL of the center spot. It is well known that the emission linewidth of a 2D electron-hole gas is a measure of the holes and electron Fermi energies which are determined by their corresponding densities ( $n_{\text{cold}}$  and  $p_{\text{cold}}$ ). Figure 2(f) shows the calculated linewidth ( $\gamma$ ) assuming a quasidegenerate 2D electron-hole gas, and is given by  $\gamma = E_f^e + E_f^h = \pi \hbar^2 (n_{\text{cold}}/m_e + p_{\text{cold}}/m_h)$ . Here,  $E_f^e$  and  $E_f^h$  are the electron and hole Fermi energies, and  $m_e$  and  $m_h$  are the electron and hole effective masses, respectively. The energy shift due to band gap renormalization also depends on  $n_{\text{cold}}$  and  $p_{\text{cold}}$ : the larger the total carrier density, the larger the emission redshift due to carrier-carrier correlations. Following Refs. [10,11], the band gap renormalization is approximated by  $E_{\text{BGR}} = E_0 - \eta (n_{\text{cold}}/m_e + p_{\text{cold}}/m_h)^{1/3}$ , and is plotted in Fig. 2(g).

Here,  $E_0$  is the QW transition energy (at zero density) and  $\eta$  is a fitting parameter. Both the calculated linewidth and energy shift agree well with the experimental results. Finally, Fig. 2(g) plots the calculated peak intensity of the center spot and ring PL as a function of power. Again, it agrees well with the experimental behavior shown in Fig. 2(d).

In addition to the above described quantitative agreement of the experiment and the model, it is also easy to understand how the qualitative trends come about. At low excitation power, we do not generate enough cold holes to substantially deplete the existing cold electron density (estimated to be  $10^{11} \text{ cm}^{-2}$  from PL linewidth). Thus, we should see PL corresponding to recombination in the presence of a high density of free charge carriers which should be broad, redshifted, and asymmetric, as we indeed observe [see Fig. 1(g)]. Increasing excitation power, the depletion of electrons becomes more significant, leading to a reduction of the excess electron density with only a small increase of holes. This lower density leads to a decrease in linewidth and a smaller redshift of the center spot. As the power is further increased, the center spot is completely depleted of electrons and the ring starts to appear. At this point, the total carrier density at the center is around  $2 \times 10^{10} \text{ cm}^{-2}$ , and correspondingly the spectral lines are narrower and less redshifted [see Fig. 1(h)]. Increasing the power still further will start to build up a large hole density in the center spot. The increase of charge carriers then reverses the previous trend, making the central spot once again broad, asymmetric, and redshifted [see Fig. 1(i)]. In contrast, the total carrier density at the ring ( $\sim 2 \times 10^{10} \text{ cm}^{-2}$ ) remains nearly independent of the excitation power, and therefore no change in its linewidth and energy position is observed. At this low density, the emission from the ring appears excitonic.

The ability of our model to describe the various experimental results strongly supports the validity of the physical picture presented above. The agreement of the experiment and theory is impressive—particularly given the very crude nature of the theoretical model. Furthermore, the qualitative trends of the model are quite independent of the precise values of the input parameters.

We are now in a good position to answer the questions posed at the beginning of this Letter. According to our model, the particles that are being transported are free carriers and no additional excitonic transport mechanism is necessary to explain our experimental data. Nonetheless, it seems that the ring emission is due to excitonic recombination (as is the center spot for excitation powers close to the threshold power for ring creation). The actual thermodynamic state of the exciton gas in the ring remains an open question. It was hypothesized in Refs. [1,2] that the exciton gas is statistically degenerate. This is not excluded by our model (see below). In fact, our model predicts a carrier density of  $\sim 2 \times 10^{10} \text{ cm}^{-2}$ , which is of the order of the Kosterlitz-Thouless 2D transition density of a superfluid state at  $T = 2 \text{ K}$ . (The data

of Figs. 1 and 2, however, are performed at higher temperatures.) As for the driving force, diffusion of free carriers seems to sufficiently account for the observed effects, and any long range Coulomb interactions will be screened out by the  $n^+$  conducting layers. However, the Coulomb term may be important in understanding the periodic beadlike structure reported in Ref. [1], which could possibly be due to competition between repulsion of like charges and attraction of opposite charges.

An intriguing prediction of the model is that the macroscopic charge separation and therefore the ring emission persist for an extremely long time compared to the center spot lifetime after the laser excitation is turned off. This behavior is shown in Fig. 3(e), where the ring lifetime is longer than  $1 \mu\text{s}$ . In comparison, the center spot decays after less than  $1 \text{ ns}$  [Fig. 3(f)]. While the center spot lifetime is determined by the free carrier recombination time, the ring lifetime is determined by a slow carrier diffusion, driven by the carrier density gradients in the plane. This long lifetime is consistent with time-resolved measurements of Ref. [2], which reported a ring PL lifetime longer than  $260 \text{ ns}$ . This suggests that excitons being formed in the ring should be well thermalized (as is also suggested by their narrow emission linewidth) because the carriers should have had plenty of time to cool from their hot optical creation. This should be a very good method of forming cold, high density excitons, opening up opportunities for studying their quantum statistics at low temperatures. Moreover, this is the first time that a boundary between two types of charged plasmas and a spontaneous pattern formation in a charged system have been optically induced and identified.

This work has been partially supported by the National Science Foundation and the Department of Energy. We thank Phil Platzman, Girsh Blumberg, Nikolai Zhitenev, Rafi de Picciotto, Chandra Varma, and Peter Littlewood for helpful discussions.

- 
- [1] L.V. Butov, A.C. Gossard, and D.S. Chemla, *Nature* (London) **418**, 751 (2002).
  - [2] D. Snoke *et al.*, *Nature* (London) **418**, 754 (2002).
  - [3] D. Snoke *et al.*, *Solid State Commun.* **127**, 187 (2003).
  - [4] D. Snoke, S. Denev, and Y. Liu (unpublished).
  - [5] I.V. Kukushkin *et al.*, *Phys. Rev. B* **40**, 4179 (1989).
  - [6] A detailed description of the sample and model parameters is given in Rapaport *et al.*, cond-mat/0308150.
  - [7] G. Ramon *et al.*, *Phys. Rev. B* **65**, 085323 (2002).
  - [8] *Properties of Aluminum Gallium Arsenide*, edited by S. Adachi (INSPEC, London, U.K., 1993).
  - [9] J. Shah, *Hot Carriers in Semiconductor Nanostructures: Physics and Applications* (Academic Press, New York, 1992).
  - [10] G. Tränkle *et al.*, *Phys. Rev. B* **36**, 6712 (1987).
  - [11] S. Schmitt-Rink *et al.*, *Solid State Commun.* **52**, 123 (1984).